Impact of Strain on Tunneling Current and Threshold Voltage in III-V Nanowire TFETs

Impact of Strain on Tunneling Current and Threshold Voltage in III-V Nanowire TFETs

Michele Visciarelli, Elena Gnani, *Member, IEEE*, Antonio Gnudi, *Member, IEEE*, Susanna Reggiani, *Member, IEEE*, and Giorgio Baccarani, *Life Fellow, IEEE*

***Abstract*—A simulation study on the effects of different strain configurations on n-type III-V-based nanowire Tunnel-FETs is presented, with the aim to determine optimal strain conditions to enhance device performance. We find that both biaxial tensile, and uniaxial compressive stress, shift up the valence band. Biaxial stress, however, lowers the conduction band as well, thus providing the largest reduction of the energy bandgap. Instead, the gap variation is limited for biaxial compressive and uniaxial tensile strains. Moreover, for these strain conditions, the lowest conduction subband is not connected to the highest valence subband via the imaginary wave vector but to a lower one. This leads to an "effective" band gap higher than expected, which reflects into a large threshold increase and a degradation of the on-state current.**

***Index Terms*—Tunnel FETs, strain, nanowire, III-V materials, NEGF**

I. Introduction

TUNNEL FETs are one of the most promising device architectures which could possibly overcome the fundamental MOSFETs limit of the inverse subthreshold slope SS ≥ 60 mV/dec. A steeper SS is in fact an essential prerequisite for an aggressive supply-voltage scaling below 0.5 V in CMOS technology [1]–[3]. This device architecture, however, is still affected by a number of drawbacks still unsolved: 1) achieving a higher on-state current $I_{\rm ON}$; 2) suppressing ambipolar effects, and, 3) dealing with the superlinear onset and high saturation voltage of the output characteristics [4].

One possible way to tackle these limits is the introduction of strain [5]–[7]. It has been recently asserted that a substantial performance improvement of homojunction InAs nanowire (NW) TFETs can be achieved using appropriate stress conditions, namely, biaxial tensile, and uniaxial compressive stress [8], [9]. Both conditions do in fact narrow the bandgap, thereby enhancing the tunneling probability.

In this letter, the scope of the investigation is widened to include additional stress conditions, namely the biaxial compressive and uniaxial tensile stresses. The latter exhibits an anomalous behavior, as it still narrows the bandgap, albeit to a lesser extent than the opposite condition proposed in [8]. It is thus of interest clarifying such an anomaly. In doing so, we found that an analysis based uniquely on bandgap narrowing can be misleading, because, in some cases, the lowest conduction subband is not connected to the highest valence band via the imaginary branch of the wave vector. This leads to an "effective" band gap, that is somewhat wider than the real one, causing a decrease of $I_{\rm ON}$ and a large threshold increase. This is exactly the case for biaxial compressive and uniaxial tensile conditions. These results can be of technological interest and help avoid unintentional strain conditions that could degrade, rather than improve, the device performance. Moreover, if an optimization procedure would be carried out to find the best channel material for Tunnel FETs in terms of bandgap and effective mass [10], in the presence of strain the "effective" bandgap should be considered instead of the material energy gap.

The authors are with the E. De Castro Advanced Research Center on Electronic Systems, University of Bologna, Bologna 40136, Italy (e-mail: michele.visciarelli2@unibo.it.).

This work has been supported by the EU Grant No. 619509 (E2Switch).
Manuscript received DATA; revised DATA.

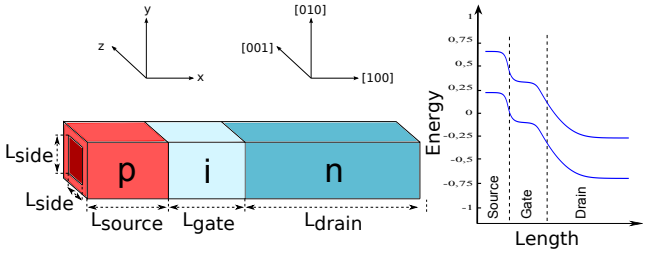

Fig. 1. Left: sketch of the simulated nanowire TFETs (not to scale). The coordinate system is also shown, together with the crystallographic one. The nanowire transport orientation is [100]. Right: profile of the first conduction and valence subbands for the $5 \times 5\,\mathrm{nm}^2$ InAs nanowire along the transport direction at $V_{\rm DS}$=0.3 V.

II. Device under study and physical model

Calculations have been performed for different III-V-based nanowire Tunnel-FETs. As an example, results obtained for an n-type InAs homojunction gate-all-around (GAA) reference device will be presented. The device structure is shown in Fig. 1, with $L_{side} = 5$ nm, $L_{source} = 20$ nm, $L_{gate} = 20$ nm and $L_{drain} = 40$ nm, source doping $N_S = 5 \times 10^{19}$ cm^{-3}, drain doping $N_D = 1 \times 10^{18}$ cm^{-3}, and $T_{ox} = 1$ nm of SiO_2. The drain doping is much lower than the source one to limit the ambipolar effect related to channel-drain band lineup (see subband profiles in Fig. 1-right). Therefore, a longer drain region is necessary to ensure charge neutrality at the drain contact. The nanowire transport orientation is [100] and the nanowire sides are along the [010] and [001] directions.

The in-house simulator employed for the present investigation is based on a 4-band $\mathbf{k} \cdot \mathbf{p}$ Hamiltonian [11], to accurately model band structure effects. The 4-band model has been used instead of the 8-band one to reduce the computational burden and to increase the readibility of the band structure. A

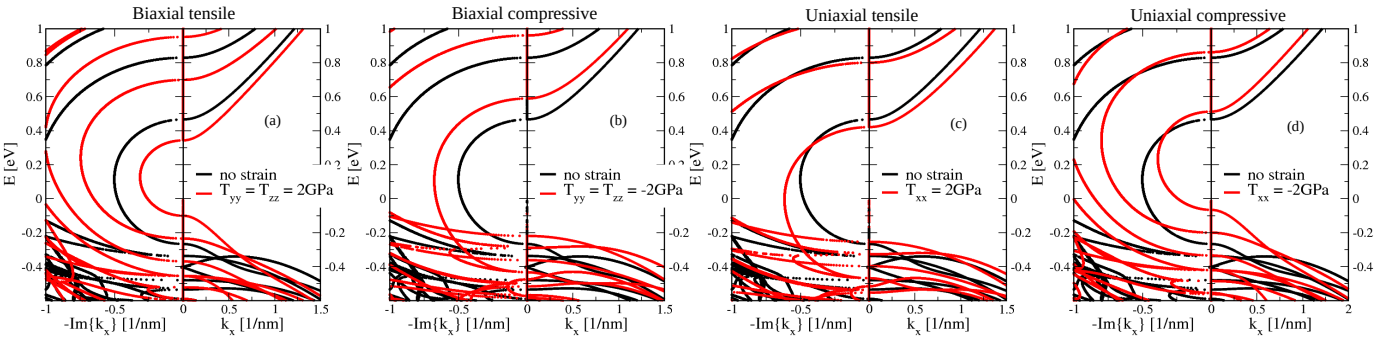

Fig. 2. Energy dispersion for the $5 \times 5\,\mathrm{nm}^2$ InAs nanowire: (a) biaxial tensile $T_{yy} = T_{zz} = 2\,\mathrm{GPa}$; (b) biaxial compressive $T_{yy} = T_{zz} = -2\,\mathrm{GPa}$; (c) uniaxial tensile $T_{xx} = 2\,\mathrm{GPa}$; (d) uniaxial compressive $T_{xx} = -2\,\mathrm{GPa}$. Biaxial tensile strain shifts up the valence band and lowers the conduction band, giving the largest gap reduction among all cases. For the uniaxial tensile and biaxial compressive strain, the imaginary wave vector does not connect the lowest conduction subband with the highest valence subband, but with a valence subband at ≈ 0.2 eV below the first one.

TABLE I
BAND GAP, "EFFECTIVE" BAND GAP, AND ELECTRON (HOLE) EFFECTIVE MASS OF THE FIRST CONDUCTION (VALENCE) SUBBAND FOR THE UNSTRAINED, BIAXIAL AND UNIAXIAL STRESS CONDITIONS AS IN FIG. 2. THE EFFECTIVE MASS VALUES ARE EVALUATED FROM THE REAL BRANCH OF THE $E(k)$ SHOWN IN FIG. 2.

	E_G [eV]	"effective" E_G [eV]	m_e $[m_0]$	m_h $[m_0]$
Unstrained	0.735	–	0.057	0.057
Biax. tens.	0.45 (−39%)	–	0.036 (−37%)	0.033 (−42%)
Biax. comp.	0.81 (+10%)	1.0 (+25.5%)	0.077 (+35%)	0.33 (+226%)
Uniax. tens.	0.67 (−8%)	0.88 (+31%)	0.072 (+26%)	0.33 (+226%)
Uniax. comp.	0.58 (−21%)	–	0.043 (−24.5%)	0.039 (−31%)

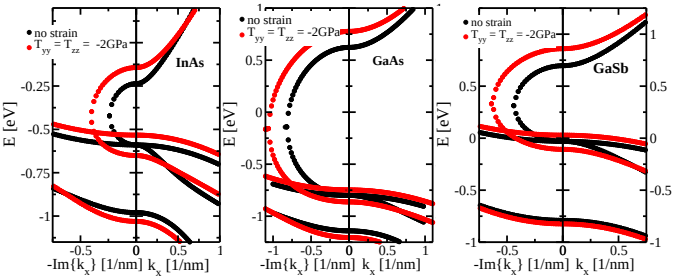

Fig. 3. Energy dispersion for bulk InAs (left), GaAs (center), and GaSb (right) under biaxial compressive strain $T_{yy} = T_{zz} = -2\,\mathrm{GPa}$. For all of them, the first conduction band is connected via the imaginary wave vector with the second valence band. The 8-band model has been used here.

ballistic and full 3D transport model is adopted based on the Non Equilibrium Green Function (NEGF) formalism. Strain is taken into account following Bahder's theory [12], [13], according to which a strain-dependent matrix is added to the standard $\mathbf{k} \cdot \mathbf{p}$ matrix. Material parameters are taken from [14] (zinc-blende crystal structure is assumed), and spurious solutions are eliminated using the procedure proposed in [15].

III. EFFECT OF STRAIN ON THE BAND STRUCTURE

Fig. 2 reports the calculated energy dispersion relationship under different strain conditions: biaxial tensile ($T_{yy} = T_{zz} = 2\,\mathrm{GPa}$), biaxial compressive ($T_{yy} = T_{zz} = -2\,\mathrm{GPa}$), uniaxial tensile ($T_{xx} = 2\,\mathrm{GPa}$), and uniaxial compressive ($T_{xx} = -2\,\mathrm{GPa}$). Uniaxial strain has been applied along the transport direction of the device, whereas biaxial strain has been applied to the device cross section, hence perpendicularly to the transport direction. All non explicitly mentioned stress components are set to zero. Both biaxial tensile and uniaxial compressive stresses shift up the valence band, but biaxial stress also lowers the conduction band and, thus, achieves the largest reduction of the band gap and of the imaginary wave-vector in the gap. The InAs nanowire band gap is reduced from $\approx 0.73\,\mathrm{eV}$ to about $0.45\,\mathrm{eV}$ with biaxial tensile stress, and the electron and hole effective masses decrease roughly by the same factor (see Table I). Note that the effective mass values are evaluated from the real branch of the dispersion relationship $E(k)$ shown in Fig. 2. For biaxial compressive strain, instead, the band gap slightly increases by 70 meV, while, for uniaxial tensile strain, E_G, extracted from the real part of the $E(k)$, unexpectedly decreases by 60 meV. From Fig. 2 we can clearly see that the lowest conduction subband is not connected to the highest valence subband via the imaginary branch of the wave vector. It is connected instead to a valence subband ≈ 0.2 eV below the highest valence subband. This leads to an "effective" band gap higher than that inferred from the inspection of the real branch of $E(k)$ (see Table I).

It is worth noting that this effect takes place also for bulk and thin body devices, and is independent of the device cross section [16]. A similar behavior is found for other III-V materials, such as GaSb and GaAs. For example, Fig. 3 shows the $E(k)$ for bulk InAs (left), GaAs (center), and GaSb (right) under biaxial compressive strain $T_{yy} = T_{zz} = -2\,\mathrm{GPa}$. For all of them, the first conduction band is connected via the imaginary wave vector with the second valence band.

IV. TFET SIMULATION RESULTS

The different strain configurations, shown in Fig.2, have a strong impact on the current-voltage characteristics. Fig. 4 compares I-V curves for the $5 \times 5\,\mathrm{nm}^2$ InAs nanowire TFET for different stress conditions. The current is normalized with respect to the nanowire side, and all simulations are carried out at $V_{\mathrm{DD}} = 0.3\,\mathrm{V}$. In Fig. 5 the metal gate work function has been adjusted to have $\mathrm{I_{OFF}}$ = 1 nA/μm at $V_{\mathrm{GS}} = 0\,\mathrm{V}$. Biaxial tensile strain reduces the threshold voltage V_T and increases

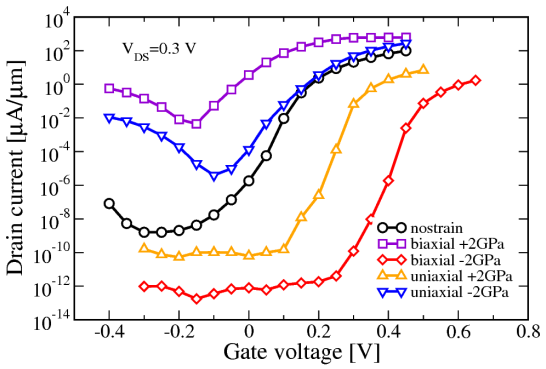

Fig. 4. $I_{\rm DS}$ versus $V_{\rm GS}$ curves at $V_{\rm DS} = 0.3\,$V for the InAs homojunction device with different strain types. The current is normalized with respect to the nanowire side. There are two unfavorable strain configurations which give a small $I_{\rm ON}$ and an unusual behavior: uniaxial tensile and biaxial compressive strain.

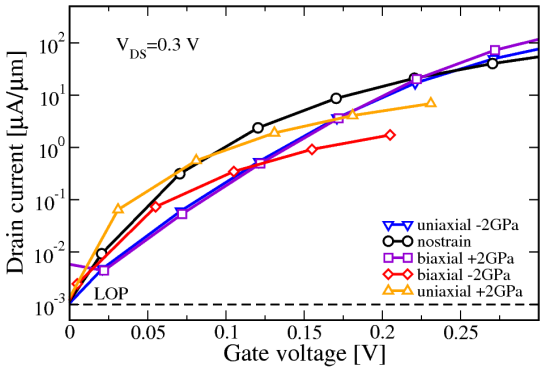

Fig. 5. I_{DS} versus V_{GS} curves at $V_{DS} = 0.3\,$V for the InAs homojunction device with different strain types. The current is normalized with respect to the nanowire side. The metal gate work function has been adjusted to to have $\rm I_{OFF}$ = 1 nA/μm at $V_{\rm GS} = 0\,$V.

the on-current due to bandgap narrowing. The drawback is the leakage current increase due to ambipolarity (above 5 nA/μm) and a substantial slope degradation due to the higher degeneracy caused by the effective-mass decrease (see Table I) [4]. A similar trend can be seen for uniaxial compressive strain, albeit with a smaller V_T change. In this case, only the valence band is shifted up, while the conduction band minimum is nearly unchanged.

For the other two stress cases (biaxial compressive ad uniaxial tensile), the strain effect is a large on-state current decrease with respect to the corresponding unstrained value, even if the band gap is slightly affected. Moreover, a dramatic increase of the threshold voltage is obtained. This unusual behavior seen for the biaxial compressive and uniaxial tensile strain can be explained by plotting the current spectrum on top of the subband profile vs. position. The uniaxial compressive and tensile cases are compared in Fig. 6. Two different gate voltages are applied for the two strain conditions in order to obtain a similar energy window for tunneling. In the uniaxial compressive case (Fig. 6 left) tunneling occurs in the whole energy window between the source valence band and the channel conduction band. On the contrary, for uniaxial tensile strain, tunneling occurs within a reduced energy window,

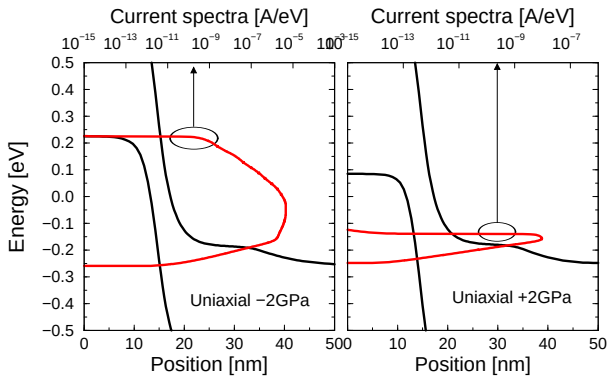

Fig. 6. Subband profile and current spectrum as a function of energy for the InAs homojunction, for uniaxial compressive at $V_{\rm GS} = 0.2$V (left) and uniaxial tensile strain at $V_{\rm GS} = 0.4$V (right). For the uniaxial compressive case, the current flows at all energies for which there are available states both in the source and in the channel. In the uniaxial tensile case the current is negligible up to 0.2 eV below the first valence subband in the source.

whose upper limit is about 0.2 eV below the first valence subband in the source. This is exactly the energy difference between the edges of the highest valence subband and the one connected to the lowest conduction subband via the imaginary wave vector (see Fig.2 (c)). This leads to an "effective" band gap $\approx 0.2\,$eV larger than expected, and to a reduced $I_{\rm ON}$.

V. Conclusion

In this work we have investigated the effects of different strain configurations on n-type III-V-based nanowire TFETs, namely biaxial in the cross-section and uniaxial in the transport direction, with the aim of finding optimal strain configurations to enhance the device performance. To this purpose, following Bahder's theory, the in-house developed simulator based on a 4-band $\mathbf{k}\cdot\mathbf{p}$ Hamiltonian has been properly extended to take into account the effects of strain. Comparison among dispersion relationships under different strain conditions shows that biaxial tensile and uniaxial compressive strain decrease the bandgap of the material, which leads to a better $I_{\rm ON}$ current, but also to a degraded subthreshold slope and a generally-worse $I_{\rm OFF}$. On the other hand, uniaxial tensile and biaxial compressive strains do not reduce the band gap significantly. However, for these two strain configurations, the main effect is that the lowest conduction subband and the highest valence subband are not connected via the imaginary wave vector: the first conduction band is connected instead to a valence subband $\approx 0.2\,$eV below the topmost valence subband. This leads to an "effective" gap which is 0.2 eV larger than the one inferred looking only at the real-part of the dispersion relationship E(k). Hence, the I-V curves show an unexpected V_T increase and $I_{\rm ON}$ degradation. To summarize, taking advantage of stress requires a very tight control of the fabrication processes, which is required to prevent unintentional strain conditions which can deteriorate, rather than improve, the overall device performance.

REFERENCES

[1] A. Seabaugh and Q. Zhang, "Low-voltage tunnel transistor for beyond CMOS logic". *Proc. IEEE*, vol. 98, no. 12, pp. 2095-2110, Dec. 2010. DOI: 10.1109/JPROC.2010.2070470

[2] A. M. Ionescu and H. Riel, "Tunnel field-effect transistors as energy-efficient electronic switches". *Nature*, vol. 479, no. 7373, pp. 329-337, Nov. 2011. DOI: 10.1038/nature10679

[3] H. Lu and A. Seabaugh, "Tunnel field-effect transistors: state-of-the-art". *J. Electron Device Soc.*, vol. 2, no. 4, Jul. 2014. DOI: 10.1109/JEDS.2014.2326622

[4] E. Gnani, A. Gnudi, S. Reggiani and G. Baccarani, "Drain-conductance optimization in nanowire TFETs by means of a physics-based analytical model". *Solid State Electronics*, vol. 84, pp. 96-102, Mar. 2013. DOI: 10.1016/j.sse.2013.02.012

[5] S. Brocard, M. Pala and D. Esseni, "Design options for hetero-junction tunnel FETs with high on current and steep sub-threshold voltage slope". in *Proc. IEEE IEDM*, pp. 5.4.1-5.4.4, Dec. 2013. DOI: 10.1109/IEDM.2013.6724567

[6] P. -F. Guo, L. -T. Yang, Y. Yang, L. Fan, G. -Q. Han, G. S. Samudra and Y. -C. Yeo, "Tunneling field-effect transistors: effect of strain and temperature on tunneling current". *IEEE Electron Device Lett.*, vol. 30, no. 9, Sep. 2009. DOI: 10.1109/LED.2009.2026296

[7] P. Wiegle, L. Czornomaz, D. Caimi, N. Daix, M. Sousa, J. Fompeyrine and C. Rossel, "III-V heterostructure-on-insulator for strain studies in n-InGaAs channels". in *Proc. 14th Int. Conf. Ultimate Integr. Silicon (ULIS)*, pp. 45-48, Mar. 2013. DOI: 10.1109/ULIS.2013.6523487

[8] F. Conzatti, M. G. Pala, D. Esseni, E. Bano and L. Selmi, "Strain-induced performance improvements in InAs nanowire tunnel FETs". *IEEE Trans. Electron Devices*, vol. 59, no. 8, pp. 2085-2092, Aug. 2012. DOI: 10.1109/TED.2012.2200253

[9] F. Conzatti, M. G. Pala, D. Esseni, and E. Bano, "Investigation of localized versus uniform strain as a performance booster in InAs tunnel-FETs". *Solid State Electronics*, vol. 88, pp. 49-53, Aug. 2013. DOI: 10.1016/j.sse.2013.04.005

[10] H. Ilatikhameneh, G. Klimeck, and R. Rahman, "Can Homojunction Tunnel FETs Scale Below 10 nm?", *IEEE Electron Device Lett.*, vol. 37, no. 1, pp. 115-118, Jan. 2016. DOI: 10.1109/LED.2015.2501820

[11] E. Baravelli, E. Gnani, R. Grassi, A. Gnudi, S. Reggiani and G. Baccarani, "Optimization of n- and p-type TFETs integrated on the same InAs/AlxGa1-xSb technology platform". *IEEE Trans. Electron Devices*, vol. 61, no. 1, pp. 178-184, Jan. 2014. DOI: 10.1109/TED.2013.2289739

[12] T. Bahder, "Eight-band k*p model of strained zinc-blende crystals". *Phys. Rev. B*, vol. 41, no. 17, pp. 11992-12001, Feb. 1990. DOI: 10.1103/PhysRevB.41.11992

[13] T. Bahder, "Erratum: Eight-band k*p model of strained zinc-blende crystals". *Phys. Rev. B*, vol. 46, p. 9913, Feb. 1992. DOI: 10.1103/PhysRevB.46.9913

[14] I. Vurgaftman, J. R. Meyer and L. R. Ram-Mohan, "Band parameters for III-V compound semiconductors and their alloys". *J. Appl. Phys.*, vol. 89, no. 11, pp. 5815-5875, Feb. 2001. DOI: 10.1063/1.1368156

[15] B. A. Foreman, "Elimination of spurious solutions from eight-band kp theory". *Phys. Rev. B*, vol. 56, pp. R12748-R12751, Jul. 2001. DOI: 10.1103/PhysRevB.56.R12748

[16] K. Majumdar, "Band to band tunneling in III-V semiconductors: implications of complex band structure, strain, orientation, and off-zone center contribution". *J. Appl. Phys.*, vol. 115, no. 17, pp. 174503, May 2014. DOI: 10.1063/1.4874917